# Optimal dimensions of cone and pyramid moth-eye structures for SiO<sub>2</sub> windows

CHAORAN TU,<sup>1</sup> WEI ZHANG,<sup>2</sup> JONATHAN HU,<sup>2,\*</sup> CURTIS R. MENYUK,<sup>1</sup> THOMAS F. CARRUTHERS,<sup>1</sup> L. BRANDON SHAW,<sup>3</sup> LYNDA E. BUSSE,<sup>3</sup> AND JASBINDER S. SANGHERA<sup>3</sup>

**Abstract:** We computationally investigate the transmission efficiency through moth-eye nanostructures that are fabricated on  $SiO_2$  windows in the wavelength range from 0.4 to 2  $\mu$ m. We investigated both truncated cones and truncated pyramids, and we varied the height, bottom width, and top width of these shapes in order to maximize the transmission efficiency. We found that there is no substantial difference in transmission between truncated cone and pyramid structures. Using the constraints from the current achievable experimental limits, a relatively uniform transmission coefficient of larger than 99.0% can be obtained from 0.4  $\mu$ m to 2  $\mu$ m. These transmission results are only 0.5% in absolute value lower than the transmission of a structure that is not constrained by current experimental limits.

© 2025 Optica Publishing Group under the terms of the Optica Open Access Publishing Agreement

#### 1. Introduction

Moth-eye structures are made of a biomimetic and periodic array of nanostructures on a substrate, which can reduce the Fresnel reflections by reducing the impedance mismatch of the air and the substrate [1–5]. The moth-eye structures introduce a smooth transition between one medium and another, ensuring that incident light does not encounter a sudden change in the refractive index, which would cause a strong reflection. Conventional antireflection (AR) coatings have a narrow transmission window. Multilayer AR coatings [6–8] overcome this limit by gradually varying the effective refractive index profile. Similarly, moth-eye structures include micron or nano moth-eye elements on the surface [9,10], which effectively provide a gradually varying effective refractive index profile and can also achieve broad transmission windows. Additionally, motheye structures have several important advantages over thin-film AR coatings, including single material fabrication, minimal surface preparation, environmental tolerance, surface adhesion, and self-cleaning via the lotus effect [11,12]. Additionally, it has also been shown that in many cases periodic moth-eye structures have a higher laser-induced damage threshold than do traditional AR-coated surfaces [13–17]. Moth-eye structures are currently used in many applications, including flexible display devices [18], automotive glass [11,19], fiber optics [20,21], laser systems [21–24], and photovoltaics [25–30].

In prior work, Busse et al [16] fabricated fused silica glass windows with optical transmission greater than 99.5% for wavelengths between  $0.775\,\mu m$  and  $1.35\,\mu m$ , and we have achieved a theoretical transmission larger than 99.5% over the wavelength range from  $0.5\,\mu m$  to  $2.0\,\mu m$  using moth-eye cone structures [31]. There have been many investigations of different moth-eye structure shapes for laser transmission, display, and solar cell applications [1,18,21–30,32–34]. The moth-eye structures that have been investigated are generally cones or pyramids [11] and an

<sup>&</sup>lt;sup>1</sup> Department of Computer Science and Electrical Engineering, University of Maryland Baltimore County, Baltimore, Maryland 21250, USA

<sup>&</sup>lt;sup>2</sup>Department of Electrical and Computer Engineering, Baylor University, Waco, Texas 76798, USA

<sup>&</sup>lt;sup>3</sup>US Naval Research Lab, 4555 Overlook Ave SW, Washington, DC 20375, USA

<sup>\*</sup>jonathan\_hu@baylor.edu

exploration of the theoretical performance limit of the pyramid structure has not been carried out to date. In this work, we compare moth-eye structures that are composed of either truncated cones or truncated pyramids, and we vary their heights, top widths, and bottom widths to maximize the transmission. We computationally investigate the transmission efficiency through one-layer of moth-eye nanostructures that are fabricated on  $SiO_2$  windows in the wavelength range from 0.4 to  $2 \,\mu m$ . We chose  $0.4 \,\mu m$  as the lower limit of our wavelength range because it aligns with the practical lower end of the visible spectrum in many optical applications [18,35].

The remainder of this paper is organized as follows: In Sec. 2, we introduce our computational model and the finite-difference time domain (FDTD) software that we use. In Sec. 3, we show our optimization results. In Sec. 4, we compare the optimal spectra. Finally, we conclude in Sec. 5.

#### 2. Computational model

Figure 1 shows a schematic illustration of truncated cones and truncated pyramids. The bottom width, top width, and height are denoted by b, t, and h, respectively. Due to experimental limits, we focused on moth-eye structures with a minimum top width of 0.15 μm and a maximum height of 0.6 µm. However, to determine the theoretically-obtainable maximum transmission, we also considered structures with larger heights and smaller top widths. In Fig. 2, we show a schematic illustration of our computational model. In our simulation, we calculated the transmission of a normally incident plane wave through the SiO<sub>2</sub> nanostructured surface using the FDTD software Lumerical. We previously validated our numerical model by comparison to experiments and demonstrated good agreement [24,31,36]. In our FDTD simulations, we use the refractive index for SiO<sub>2</sub> using the data in Refs. [37–39]. To accurately resolve the fine features of the cone or pyramid nanostructure, we used a minimum spatial resolution of 5 nm in our simulations, and we verified the convergence of the results in all cases. We took advantage of the hexagonal symmetry of the structure and periodicity of the optical field to use the computational grid that we show in Fig. 2, which consists of a single unit cell in the x- and y-directions. The unit cell has dimensions  $S_x = 1.0 \,\mu\text{m}$ ,  $S_y = \sqrt{3}S_x = 1.732 \,\mu\text{m}$ , which is consistent with [16]. The reflection monitor was placed 2.0 µm above the moth-eye structure, while the transmission monitor was placed 1.0 µm below it. We used 1 µm perfectly matched layers (PMLs) at both the top and bottom boundaries, located 1.0 µm away from the respective monitors. The light source used in the FDTD simulations is a broadband pulsed light that covers a wavelength range of 0.4 µm to 2 µm. The pulse has a temporal width of 2.7 fs and a spectral bandwidth of 600 THz. We calculated transmission and reflection spectra by taking a Fourier transform of the time-domain flux through surfaces lying just below the moth-eye structure and just above the plane wave source.

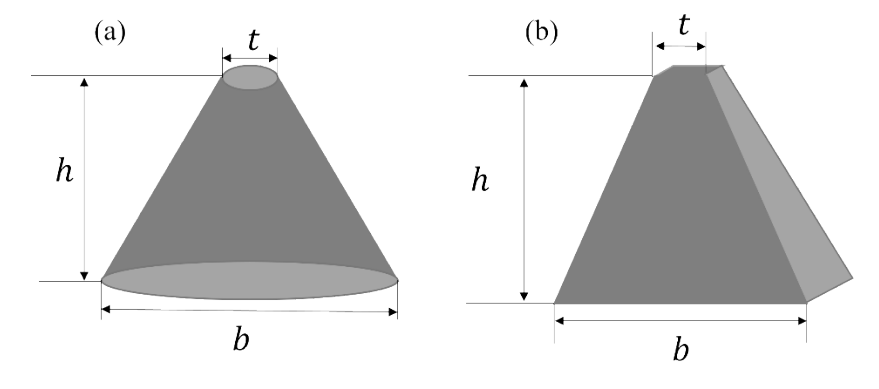


**Fig. 1.** Different shapes used in the moth-eye structure: (a) the truncated cone and (b) the truncated pyramid.

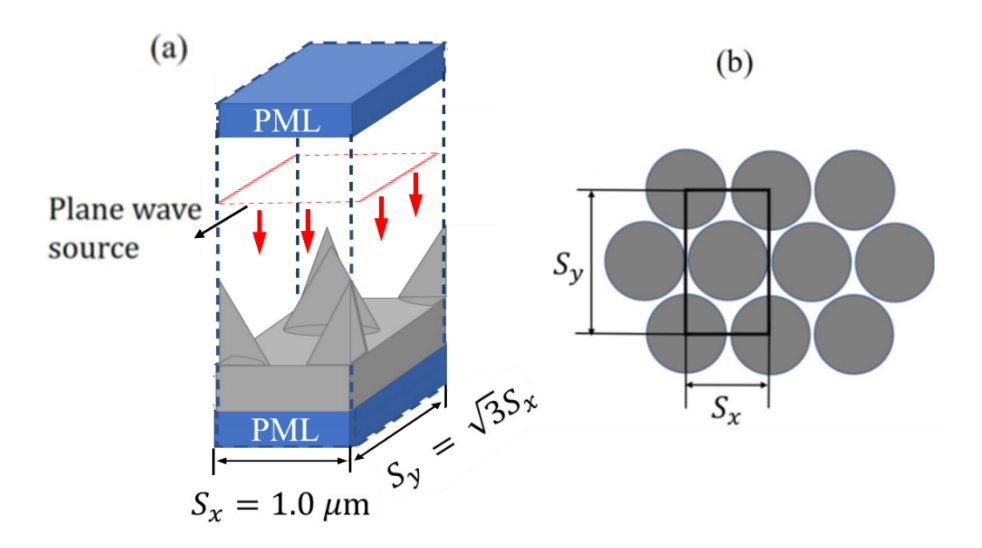


Fig. 2. Schematic view of silica moth-eye structure: (a) A three-dimensional view of the computational unit cell. (b) A top view showing a unit cell.

#### 3. Results

We used  $h = 0.6 \,\mu\text{m}$ ,  $b = 0.95 \,\mu\text{m}$ , and  $t = 0.15 \,\mu\text{m}$  as our baseline parameters. The values of h and t correspond to the achievable experimental limits. In Fig. 3, we compare the transmission spectra for two orthogonal polarizations with these baseline parameters. The polarization angle in Fig. 3 refers to the angle between the electric field direction and the x-axis. The moth-eye structures with cones are strictly hexagonally symmetric, so that the transmission has no polarization dependence [31]. By contrast, the square cross-section of the pyramids breaks the symmetry of the structures and introduces a small but negligible polarization dependence. The grey dotted line indicates the transmission through a bare flat surface. For simplicity, the remainder of our results are all obtained with a polarization angle of 0°. We see that all transmission curves for moth-eye structures show dips that we attribute to resonances with the periodic structures [22]. Similar resonant dips appear in all cases as we modify the structure parameters, but the location of the resonances depends sensitively on these parameters. In an experimental setting, where the structure parameters cannot be precisely controlled, it seems likely that these sharp dips would be smoothed out.

#### 3.1. Bottom width

In Fig. 4, we show the transmission spectra for different values of the bottom width b for both truncated cones and pyramids. We considered the truncated cones, and we allowed b to vary from 0.15 µm to 0.95 µm, which is within the range that can be fabricated. Next, we considered truncated pyramids, and we allowed b to vary from  $0.15 \,\mu m$  to  $0.8 \,\mu m$ .

For the truncated cone structures, Fig. 4(a) shows that the transmission increases in the entire wavelength range by about 0.03 when the bottom width b of the truncated cones increases from 0.15 μm to 0.95 μm. For the truncated pyramid structures, Fig. 4(b) shows that the transmission generally increases in the entire wavelength range by about 0.03 when the bottom width b of the truncated pyramids increases from  $0.15 \,\mu m$  to  $0.8 \,\mu m$ . We observe that the results are similar for truncated cone and pyramid structures.

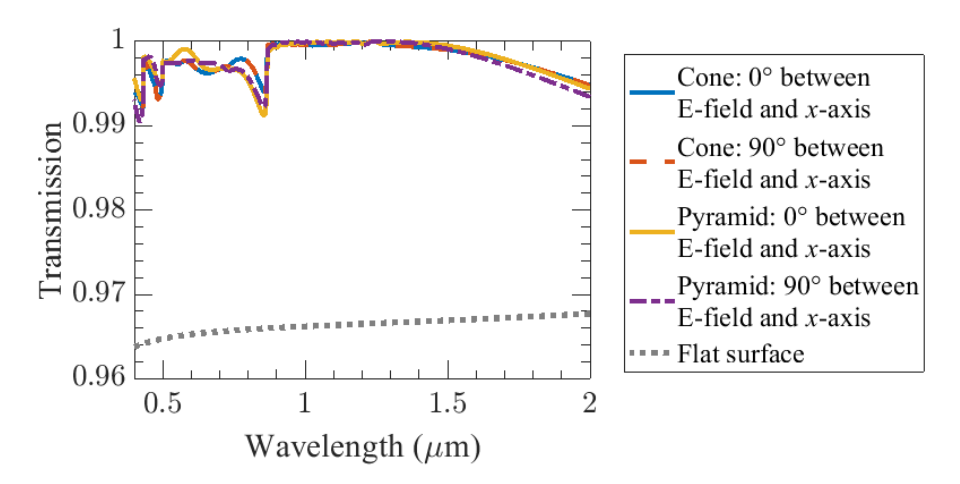


**Fig. 3.** Transmission spectra of truncated cones and pyramids with normally incident light and with polarization angles of  $0^{\circ}$  and  $90^{\circ}$ .

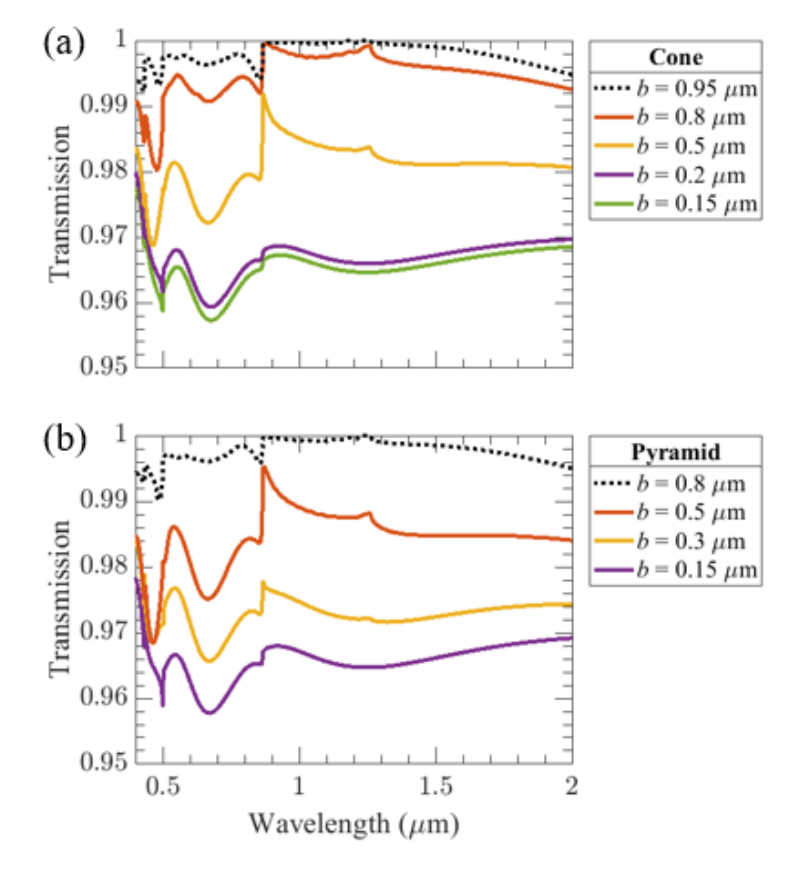


**Fig. 4.** Transmission spectra when varying the bottom width b of (a) the truncated cones ( $t=0.15~\mu m$  and  $h=0.6~\mu m$ ) and (b) the truncated pyramids ( $t=0.15~\mu m$  and  $h=0.6~\mu m$ ). The black dashed line corresponds to the currently achievable experimental limit of b=0. 95  $\mu m$  for cone structures and  $b=0.8~\mu m$  for pyramid structures.

## 3.2. Top width

In Fig. 5, we show the transmission spectra for different values of the top width t with truncated cones and pyramids. For the truncated cone structures, Fig. 5(a) shows that the transmission spectrum decreases in the entire wavelength range by about 0.02, when the top width t of the truncated cones increases from 0 to 0.95  $\mu$ m. We also find that if we reduce the top of the cone to 0.15  $\mu$ m, we almost reach the theoretically optimal transmission spectrum with t=0. For the truncated pyramid structures, Fig. 5(b) shows that the transmission spectrum decreases in the entire wavelength range by about 0.02 when the top width t of the truncated pyramids increases from 0 to 0.8  $\mu$ m. We also find that structures with t=0.15  $\mu$ m have a transmission spectrum that is close to the optimal transmission spectrum that is achieved for the top width t=0  $\mu$ m for the pyramids.

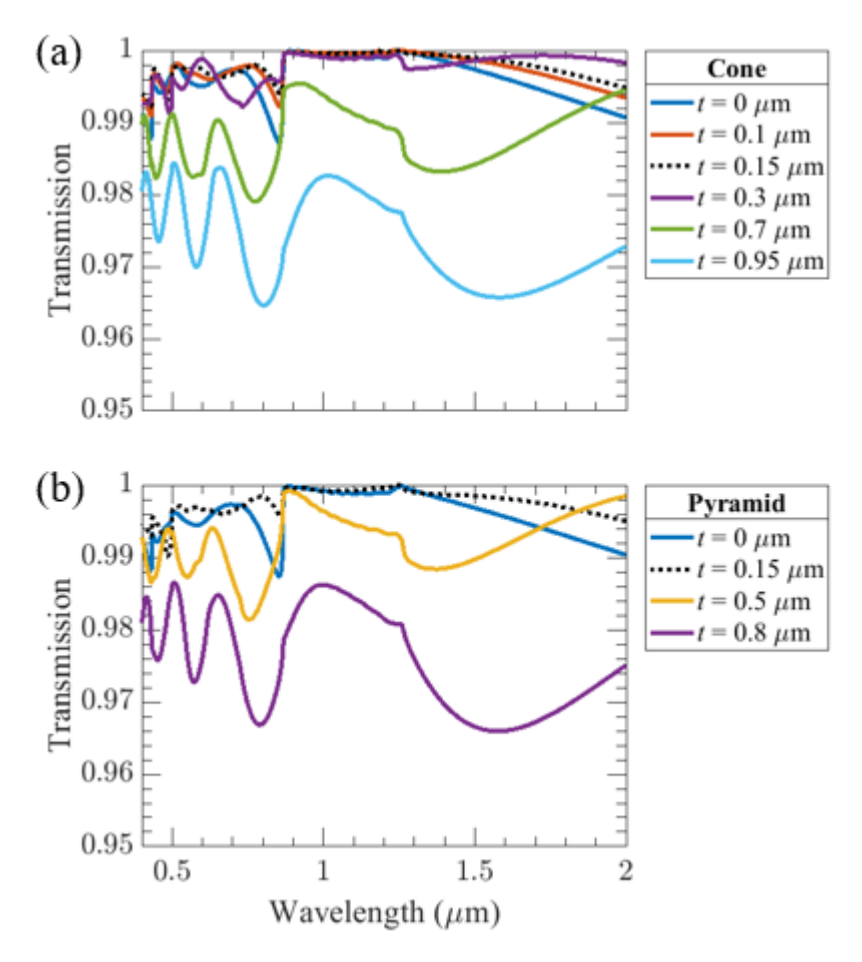


**Fig. 5.** Transmission spectra when varying the top width t of (a) the truncated cones ( $b = 0.95~\mu m$  and  $h = 0.6~\mu m$ ) and (b) the truncated pyramids ( $b = 0.8~\mu m$  and  $h = 0.6~\mu m$ ). The black dashed line in each plot corresponds to the currently achievable experimental limit of  $t = 0.15~\mu m$ .

### 3.3. Height

In Fig. 6, we show the transmission spectra for different values of the height h with truncated cones and pyramids. For both structures, we allowed h to vary between  $0.2 \,\mu m$  and  $1.6 \,\mu m$ . To

determine the theoretically achievable optimum, we also allowed h to be larger than 1.6  $\mu$ m. For the truncated cone structures, Fig. 6(a) shows that the transmission spectrum generally increases, when the height h of the truncated cones increases from 0.2  $\mu$ m to 1.6  $\mu$ m. Beyond h=0.6  $\mu$ m, there is no significant overall improvement in the transmission spectrum. For the truncated pyramid structures, Fig. 6(b) shows that the transmission spectrum generally increases when the height h of the truncated pyramids increases from 0.2  $\mu$ m to 1.6  $\mu$ m. There is no significant improvement over the entire wavelength range beyond h=0.6  $\mu$ m.

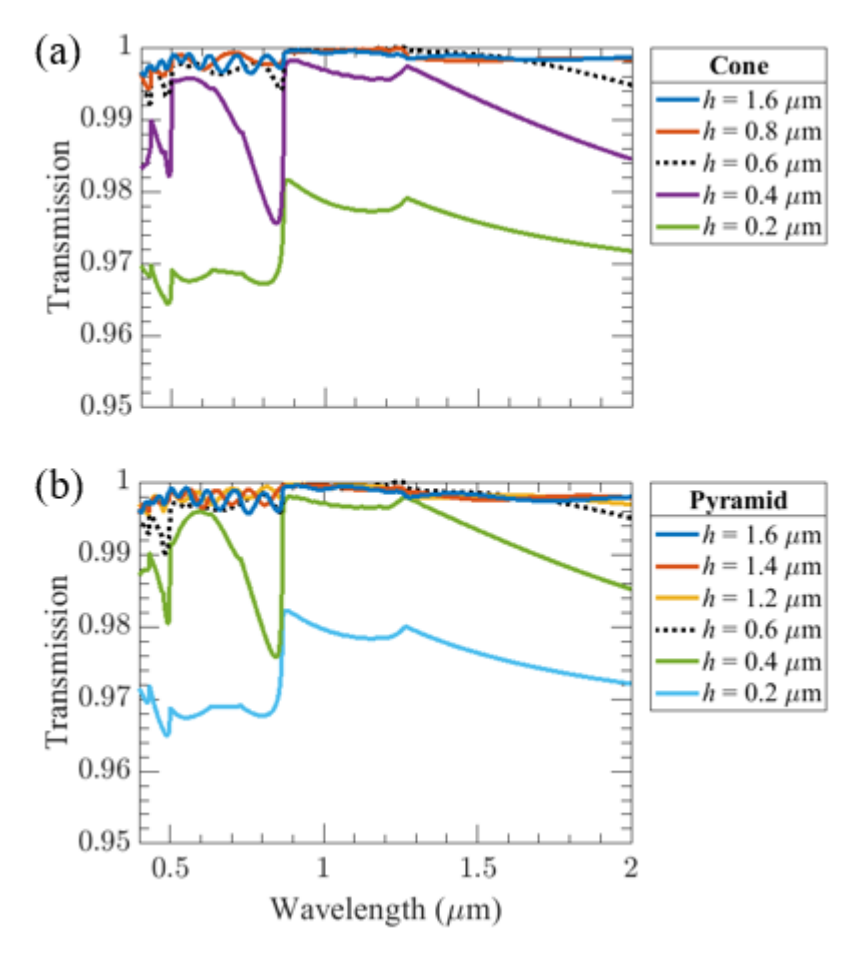


**Fig. 6.** Transmission spectra when varying the height h of (a) the truncated cones ( $t = 0.15~\mu m$  and  $b = 0.95~\mu m$ ) and (b) the truncated pyramids ( $t = 0.15~\mu m$  and  $b = 0.8~\mu m$ ). The black dashed line corresponds to the currently achievable experimental limit.

## 4. Comparison of the optimal spectra

Based on the transmission spectra, we conclude that a truncated cone moth-eye structure with a top width t that is as small as possible, a bottom width b that is as large as possible, and a cone height b that is as high as possible will have a high transmission spectrum over a wide wavelength range. In Fig. 7, we compare the transmission spectra for both truncated cone and pyramid structures. We summarize the key results in Table 1. The optimal dimensions of the truncated cone and pyramids that are consistent with the current experimental limits are:  $t = 0.15 \mu m$ ,  $b = 0.95 \mu m$ ,  $b = 0.6 \mu m$  and  $t = 0.15 \mu m$ ,  $b = 0.8 \mu m$ ,  $b = 0.6 \mu m$ , respectively. The minimum

transmission values are 99.2% and 99.0% for truncated cone and pyramid, respectively, for the entire wavelength range of interest from 0.4 to 2  $\mu$ m. The corresponding average transmission values are 99.7% and 99.6%. If we allowed the parameters to exceed the experimental limits, then the optimal parameters are t=0  $\mu$ m, b=0.95  $\mu$ m, h=1.6  $\mu$ m for truncated cone structures and t=0  $\mu$ m, b=0.8  $\mu$ m, h=2.2  $\mu$ m for truncated pyramid structures. The minimum transmission values are 99.6% and 99.5% for truncated cones and pyramids, respectively. The corresponding average transmission is 99.8% for both ideal structures. We observe that remaining within the experimental limits leads to a transmission spectrum of more than 99.0% over our entire wavelength range of interest, yielding a penalty in the transmission spectrum of less than 0.5% in an absolute value, compared to an ideal structure. We also find that there is no substantial difference in transmission between truncated cone and pyramid structures.

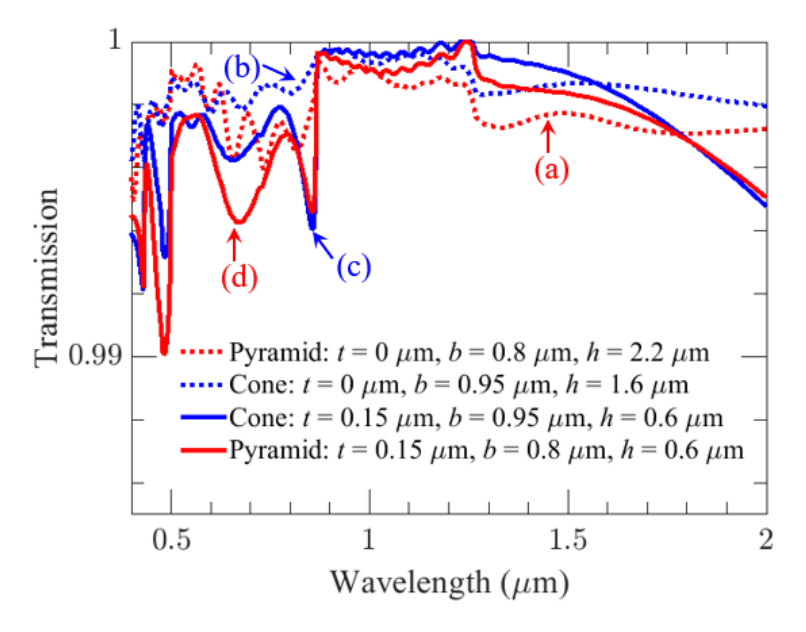


**Fig. 7.** Comparison of the transmission spectra of (a) truncated pyramids with the theoretically optimal parameters ( $t = 0 \, \mu m$ ,  $b = 0.8 \, \mu m$  and  $h = 2.2 \, \mu m$ ), (b) truncated cones with the theoretically optimal parameters ( $t = 0 \, \mu m$ ,  $b = 0.95 \, \mu m$  and  $h = 1.6 \, \mu m$ ), (c) truncated cones with the experimentally-limited optimal parameters ( $t = 0.15 \, \mu m$ ,  $b = 0.95 \, \mu m$  and  $h = 0.6 \, \mu m$ ), and (d) truncated pyramids with the experimentally-limited optimal parameters ( $t = 0.15 \, \mu m$ ,  $b = 0.8 \, \mu m$  and  $t = 0.6 \, \mu m$ ).

Table 1. Dimension and transmission of moth-eye structures

Structure Type	t (µm)	<i>b</i> (μm)	h (μm)	Minimum Transmis- sion	Average Transmis- sion
Cone	0	0.95	1.6	99.6%	99.8%
Pyramid	0	0.8	2.2	99.5%	99.8%
Truncated Cone <sup>a</sup>	0.15	0.95	0.6	99.2%	99.7%
Truncated Pyramid <sup>a</sup>	0.15	0.8	0.6	99.0%	99.6%

<sup>&</sup>lt;sup>a</sup>with current achievable experimental limits.

#### 5. Conclusion

We used the FDTD method to computationally study the transmission of light that is normally incident on a SiO<sub>2</sub> glass window with moth-eye structures that use truncated cones and pyramids. We investigated the effect of changing the top width, bottom width, and height of truncated cones and pyramids. The transmission generally increases when truncated cones and pyramids have a narrow top width, a wide bottom width, and a large height. We find that there is no substantial difference in transmission between truncated cone and pyramid structures. Within the current achievable experimental fabrication limits ( $t = 0.15 \, \mu m$ ,  $h = 0.6 \, \mu m$  with  $b = 0.95 \, \mu m$  for truncated cone structures and  $b = 0.8 \, \mu m$  for truncated pyramid structures), the optimal truncated cone and pyramid moth-eye structures have a relatively uniform transmission coefficient, which is larger than 99.0% from 0.4  $\, \mu m$  to 2  $\, \mu m$ . Using the constraints from the current achievable experimental limits, the minimum transmission is only 0.5% (in absolute value) lower than the minimum transmission of 99.5% for the theoretically optimal moth-eye structures for both truncated cones and pyramids. Although the optimal structures can give slightly higher transmission, the current fabrication limitations already give promising results close to the optimal structures.

Funding. U.S. Naval Research Laboratory (N00173-15-1- G905).

**Acknowledgements.** A portion of our computational work was carried out at UMBC High Performance Computing Facility (https://hpcf.umbc.edu). The authors would like to express their appreciation to Dr. Ergun Simsek for valuable discussions.

**Disclosures.** The authors declare no conflicts of interest.

**Data availability.** Data underlying the results presented in this paper are not publicly available at this time but may be obtained from the authors upon reasonable request.

#### References

- C. G. Bernhard and W. H. Miller, "A corneal nipple pattern in insect compound eyes," Acta Physiol. Scand. 56(3-4), 385–386 (1962).
- 2. D. G. Stavenga, S. Foletti, G. Palasantzas, *et al.*, "Light on the moth-eye corneal nipple array of butterflies," Proc. R. Soc. London, Ser. B **273**(1587), 661–667 (2006).
- 3. S. Chattopadhyay, Y. F. Huang, Y. J. Jen, *et al.*, "Anti-reflecting and photonic nanostructures," Mater. Sci. Eng. R Rep. **69**(1-3), 1–35 (2010).
- S. J. Wilson and M. C. Hutley, "The optical properties of 'moth eye' antireflection surfaces," Opt. Acta 29(7), 993–1009 (1982).
- D. Poitras and J. A. Dobrowolski, "Toward perfect antireflection coatings. 2. Theory," Appl. Opt. 43(6), 1286–1295 (2004).
- J. D. Wheeler, B. Koopman, P. Gallardo, et al., "Antireflection coatings for submillimeter silicon lenses," Proc. SPIE 9153, 91532Z (2014).
- F. Defrance, C. Jung-Kubiak, J. Sayers, et al., "1.6:1 bandwidth two-layer antireflection structure for silicon matched to the 190–310 GHz atmospheric window," Appl. Opt. 57(18), 5196–5209 (2018).
- T. Macioce, F. Defrance, C. Jung-Kubiak, et al., "Multilayer etched antireflective structures for silicon vacuum windows," J. Low Temp. Phys. 199(3-4), 935–942 (2020).
- 9. H. K. Raut, V. A. Ganesh, A. S. Nair, *et al.*, "Anti-reflective coatings: A critical, in-depth review," Energy Environ. Sci. 4(10), 3779–3804 (2011).
- Z. W. Han, Z. Wang, X. M. Feng, et al., "Antireflective surface inspired from biology: A review," Biosurface and Biotribol. 2(4), 137–150 (2016).
- D. S. Hobbs, B. D. MacLeod, and J. R. Riccobono, "Update on the development of high-performance anti-reflecting surface relief micro-structures," Proc. SPIE 6545, 65450Y (2007).
- J. Sanghera, C. Florea, L. Busse, et al., "Reduced Fresnel losses in chalcogenide fibers by using anti-reflective surface structures on fiber end faces," Opt. Express 18(25), 26760–26768 (2010).
- D. S. Hobbs, B. D. MacLeod, E. Sabatino III, et al., "Laser damage resistant antireflection microstructures in Raytheon ceramic YAG, sapphire, ALON, and quartz," Proc. SPIE 8016, 80160T (2011).
- C. Florea, L. Busse, S. Bayyab, et al., "Anti-reflective surface structures in spinel ceramic windows," in The 10th Pacific Rim Conference on Ceramic and Glass Technology (2013), paper S10-014.
- 15. L. Busse, C. Florea, L. B. Shaw, et al., "Anti-reflective surface structures for high energy laser applications," in *Annual Directed Energy Symposium* (2013), paper 13-Symp-053.
- L. E. Busse, C. M. Florea, J. A. Frantz, et al., "Anti-reflective surface structures for spinel ceramics and fused silica windows, lenses, and optical fibers," Opt. Mater. Express 4(12), 2504

  –2515 (2014).

- 17. Z. Teng, Y. Sun, F. Kong, *et al.*, "Sub-wavelength microstructures on lithium triborate surface with high transmittance and laser-induced damage threshold at 1064 nm," Opt. Laser Technol. **145**, 107487 (2022).
- G. Tan, J. Lee, Y. Lan, et al., "Broadband antireflection film with moth-eye-like structure for flexible display applications," Optica 4(7), 678–683 (2017).
- C. J. Ting, H. Y. Tsai, C. P. Chou, et al., "Optical characteristics of silver film on the moth-eye structure," J. Mech. Sci. Technol. 21(10), 1752–1755 (2007).
- J. Kulakofsky, W. Lewis, M. Robertson, et al., "Designing high-power components for optical telecommunications," Proc. SPIE 4679, 198 (2002).
- R. J. Weiblen, C. R. Menyuk, L. E. Busse, et al., "Optimized moth-eye anti-reflective structures for As<sub>2</sub>S<sub>3</sub> chalcogenide optical fibers," Opt. Express 24(10), 10172–10187 (2016).
- X. Yu, Y. Yasunaga, K. Goto, et al., "Profile control of femtosecond laser-fabricated moth-eye structures on Si substrate," Opt. Lasers Eng. 142, 106584 (2021).
- R. Contractor, G. D'Aguanno, and C. R. Menyuk, "Ultra-broadband, polarization-independent, wide-angle absorption in impedance-matched metamaterials with anti-reflective moth-eye surfaces," Opt. Express 26(18), 24031–24043 (2018).
- C. Tu, J. Hu, C. R. Menyuk, et al., "Optimized two-layer motheye structures for MgAl<sub>2</sub>O<sub>4</sub> spinel ceramic windows," Opt. Contin. 4(8), 2143–2153 (2021).
- S. A. Boden and D. M. Bagnall, "Optimization of moth-eye antireflection schemes for silicon solar cells," Prog. Photovolt: Res. Appl. 18(3), 195–203 (2010).
- J. Oh, H. C. Yuan, and H. M. Branz, "An 18:2%-efficient black-silicon solar cell achieved through control of carrier recombination in nanostructures," Nat. Nanotechnol. 7(11), 743–748 (2012).
- 27. Y. M. Song, Y. Jeong, C. Yeo, *et al.*, "Enhanced power generation in concentrated photovoltaics using broadband antireflective coverglasses with moth eye structures," Opt. Express **20**(S6), A916–A923 (2012).
- G. Cossio, E. D. Yu, S. R. Tatavarti, et al., "Omnidirectional current enhancement from laminated moth-eye textured polymer packaging for large-area, flexible III-V solar modules," IEEE J. Photovolt 11(3), 685–691 (2021).
- D. Du, Z. Xu, L. Wang, et al., "The broadband and omnidirectional antireflective performance of perovskite solar cells with curved nanostructures," Sol. Energy 224, 10–17 (2021).
- S. Ju, M. Byun, M. Kim, et al., "Fabrication of perovskite solar cell with high short-circuit current density (Jsc) using moth-eye structure of SiO<sub>x</sub>," Nano Res. 13(4), 1156–1161 (2020).
- 31. C. Tu, Z. Hu, J. Hu, *et al.*, "Optimized two-layer random motheye structures for SiO<sub>2</sub> windows," Opt. Contin. **3**(9), 1722–1731 (2024).
- 32. S. Ji, J. Park, and H. Lim, "Improved antireflection properties of moth eye mimicking nanopillars on transparent glass: flat antireflection and color tuning," Nanoscale 4(15), 4603–4610 (2012).
- 33. N. Yamada, O. N. Kim, T. Tokimitsu, *et al.*, "Optimization of anti-reflection moth-eye structures for use in crystalline silicon solar cells," Progress Photovoltaics: Res. Appl. **19**(2), 134–140 (2011).
- 34. K. M. Rosfjord, J. K. W. Yang, E. A. Dauler, *et al.*, "Nanowire single-photon detector with an integrated optical cavity and anti-reflection coating," Opt. Express **14**(2), 527–534 (2006).
- C. J. Ting, C. F. Chen, and C. P. Chou, "Subwavelength structures for broadband antireflection application," Opt. Commun. 282(3), 434–438 (2009).
- C. Tu, J. Hu, C. R. Menyuk, et al., "Optimization of random motheye structures for silica windows with normally incident light," in OSA Advanced Photonics Congress 2021, paper NoF2C.6.
- 37. I. H. Malitson, "Interspecimen comparison of the refractive index of fused silica," J. Opt. Soc. Am. 55(10), 1205–1208 (1965)
- C. Z. Tan, "Determination of refractive index of silica glass for infrared wavelengths by IR spectroscopy," J. Non-Cryst. Solids 223(1-2), 158–163 (1998).
- 39. "Refractive index of fused silica," RefractiveIndex.INFO (2024), https://refractiveindex.info/?shelf=glass&book=fused\_silica&page=Malitson.